Computational assessment of methane-air reduced chemical kinetic mechanisms for soot production studies

Cesar Celis, Luís Fernando Figueira da Silva

Computational Assessment of Methane-Air Reduced Chemical Kinetic Mechanisms for Soot Production Studies

Cesar Celis[†], Luís Fernando Figueira da Silva
Department of Mechanical Engineering, Pontifícia Universidade Católica do Rio de Janeiro
Rua Marquês de São Vicente 225, Rio de Janeiro, RJ 22451-900, Brazil

Abstract

Accurate predictions of minor chemical species and radicals are crucial for determining the production of pollutants such as soot. Reduced chemical kinetic mechanisms compromise their accuracy in favor of a lower computational cost. When using these reduced mechanisms then, it is important to assess both the accuracy of the results obtained, and the amount of computational time saved. This work describes such an assessment of seven methane-air reduced chemical kinetic mechanisms to be used for carrying out soot formation studies. The reduced mechanisms evaluated involve different numbers of chemical species and reaction steps. The assessment is carried out using partially stirred reactors, with and without in situ adaptive tabulation-based chemistry acceleration techniques, by comparing the results with detailed chemical kinetics baseline computations. In terms of accuracy, for equivalence ratios featuring significant amounts of soot (above ~1.5), and considering only those mechanisms that are readily used with the soot model utilized, the reduced mechanisms results show that major species are in general predicted reasonably well (~0-10% discrepancies). Larger discrepancies between detailed and reduced mechanisms results (~0.2-16%) are observed however when predicting minor species. The in situ adaptive tabulation technique used in this work leads to further reductions in the accuracy of the minor species predicted, i.e., to further increases in discrepancies (~0.1-7%). Regarding the computational cost, the results show that savings of up to 57% can be obtained when using the reduced mechanisms analyzed. The use of chemistry acceleration techniques results in further cost reductions ranging from 1 to 43%. Additionally, discrepancies in the predictions of soot volume fraction of the order of 4-11% are observed when using reduced mechanisms. The results obtained in this work emphasize overall the need of carefully selecting the reduced mechanism that is more suitable for a given application.

Keywords: Reduced chemical kinetic mechanisms, methane-air combustion, partially stirred reactors

1. Introduction

Designing practical combustion systems that are both efficient and environmentally friendly requires an in-depth knowledge of the tight coupling between turbulent fluctuations, chemical reactions and mixing. One way of understanding turbulence-chemistry-mixing interactions involves the use of high fidelity

[†] Corresponding author. E-mail address: Cesar.Celis@PUC-Rio.br. T: +5521 3527 1641 (C. Celis)

modeling approaches, such as those based on transported probability density function (PDF) methods [1,2]. As it usually happens when employing high fidelity models, the use of transported PDF-based approaches involves a high computational cost. The hybrid Euler/Lagrange schemes [3-11] utilized for solving the PDF transport equations are mainly responsible for the high costs observed, as they require the use of a large number (millions) of Lagrangian notional particles. In this type of hybrid schemes, the Lagrangian part evolves the reactive scalars, i.e., mixture composition, by advancing the particles in physical and composition spaces. This means that solving for a given Lagrangian particle implies integrating the chemical kinetic source terms characterizing the chemical mechanism utilized for describing the combustion process. Even for small hydrocarbons, detailed chemical kinetic mechanisms describing its oxidation may involve hundreds of chemical reactions and tens/hundreds of chemical species [12]. This is particularly true in those mechanisms developed for soot formation-related studies [13-16]. Solving all detailed mechanisms chemical kinetics at each of the tens/hundreds of millions Lagrangian particles clearly implies a huge computational time. In order to reduce this computational time then, a need appears for reduced chemical kinetic mechanisms, which are the subject of the present work.

Starting from detailed chemical kinetic mechanisms, different methodologies can be utilized for deriving reduced mechanisms. These methodologies range from classical ones, involving hypotheses about rate controlling reactions, for example, to more sophisticated ones, employing graph theory [17] or computational singular perturbation-based methods [18-21]. Over the years thus, several reduced chemical kinetic mechanisms for methane-air combustion, with different complexity levels, have been derived. Early reduced kinetic mechanisms for methane oxidation typically consist of three to four steps (reactions). Examples of these kinetic mechanisms constitute those developed by Bilger *et al.*, [22], Chen and Dibble [23], Jones and Lindstedt [24], Peters and Kee [25] and Peters and Williams [26]. Although these early mechanisms proved to be valuable at the time of their development, their applicability range is quite limited indeed. This happens because complex combustion phenomena such as flame extinction and re-ignition, and pollutant formation cannot be properly described with such a small number of steps. Reduced mechanisms for methane-air combustion derived more recently typically involve a larger number of steps, i.e., 10-20 lumped reactions [27,28]. These so-called augmented reduced mechanisms (ARMs) have been designed to be used in large scale simulations, and their applicability range is larger than that of the earlier reduced mechanisms. A reduced chemical kinetic mechanism represents, in general, the minimum set of chemical species and reaction steps that reproduces, within a specified tolerance error, the initial detailed kinetic model results. Using a reduced mechanism for a given numerical simulation implies, then, understanding the level of accuracy errors introduced, as well as the corresponding amount of computational time saved. In addition, since reduced mechanisms are derived considering a particular set of operating conditions, their accuracy it is expected to vary when these conditions change.

The main driving force behind this work is the soot formation process in methane-air combustion. Thus soot, its precursors species and oxidation agents are at the focus of the kinetic mechanisms accuracy assessment. Soot is primarily formed under fuel rich conditions, which do not necessarily correspond to those conditions accounted for when most reduced mechanisms were derived. , some of the reduced mechanisms analyzed in this work have not been evaluated yet under fuel rich, soot forming conditions. Furthermore, none of these reduced mechanisms has been derived having the formation of soot as the main

goal. It is therefore indispensable to establish the expected accuracy associated with the use of these reduced mechanisms under soot formation-related conditions, before venturing in modeling the soot formed in the experimental configurations of interest to the authors [29-31].

Notice that, at design point conditions, the amount of soot formed in combustion systems featuring methane-air flames is in general relatively small. Accordingly, methane-based flames are for instance less sooty than ethylene-based ones. Nevertheless, when covering the whole operating envelope of methane-based combustion devices, there may be conditions where the amount of soot formed is significant. Industrial gas turbine engines are a typical example where soot formation may be significant in off-design operating conditions if no control measures are considered. When equipped with conventional combustors featuring a single (and fixed) combustion zone, depending on the load level, these engines can produce a large amount of soot. Two approaches often used in practice to alleviate this problem involve the use of variable geometry and 'staged' combustion [32]. More specifically, variable geometry allows regulating the amount of air entering the primary combustion zone, and in this way, avoiding those mixture equivalence ratios leading to significant soot production. Staged combustion allows in turn creating multiple combustion zones, each of them designed to optimize particular aspects of combustion performance, including the minimization of soot emissions. The fact that (i) there are relevant applications where methane-air soot production could be important, and (ii) methane is the smallest and simplest hydrocarbon constitute the main reasons why methane-air combustion processes and their relationship to soot formation are considered in this work.

Accordingly, the main objective of this work is to assess, in terms of accuracy, computational time and suitability for carrying out soot formation studies, different methane-air reduced mechanisms in a context similar to that found in transported PDF-based hybrid Euler/Lagrange approaches. After this brief introduction (Section 1) thus, the modeling approach employed for assessing the different reduced mechanisms considered is described (Section 2). In Section 2, a particular emphasis is put on (i) the reduced mechanisms assessed, (ii) the chemical reactor-based configuration utilized, and (iii) the soot formation model used for predicting the corresponding amount of soot formed. The numerical approach utilized here is in turn highlighted in Section 3, along with a description of the chemistry acceleration technique utilized for reducing the computational time involved in the simulations. The final part of the article presents the results associated with the use of the reduced mechanisms analyzed here (Section 4), in terms of accuracy and computational efficiency, and the main conclusions (Section 5) drawn from these results.

2. Modeling Approach

The modeling methodology followed in this work for evaluating methane-air reduced mechanisms is summarized in this this section.

2.1. Reduced chemical kinetic mechanisms

Seven reduced chemical mechanisms for methane oxidation, listed in Table 1, have been evaluated in this work. The number of chemical species and reactions (steps) involved on each of these reduced mechanisms is given in Table 1. In addition, this table indicates the GRI mechanism from where the reduced mechanisms were derived, the source from where they were obtained in Chemkin format and their

corresponding references. The GRI mechanisms used as a benchmark when comparing the reduced mechanisms studied are the GRI-Mech 2.11 and 3.0 [33], denoted here as GM211 and GM30, respectively. The GRI-Mech 2.11 is a compilation of 277 elementary chemical reactions and 49 chemical species, whereas 325 chemical reactions and 53 species compose the GRI-Mech 3.0 detailed mechanism. Notice that there are two main reasons why GRI-Mech 2.11-based reduced mechanisms are analyzed here. First, the latest augmented reduced mechanisms (ARMs), ARM12 to ARM17, are based on ARMs that were derived from the GRI-Mech 2.11. Second, GRI-Mech 2.11-based reduced mechanisms such as the ARM2 are currently used for simulating turbulent flames [34,35]. Since the present study is motivated by the simulation of soot formation in turbulent flames, it is then deemed relevant to include these reduced mechanisms based on GRI-Mech 2.11 in the assessments carried out in this work.

The smallest reduced mechanism analyzed here, denoted as CHEN5, corresponds to the 5-step methane-air kinetic mechanism derived by Mallampalli *et al.* [36] for modeling the typical high pressure and fuel-lean conditions found in gas turbine combustors operating in lean premixed mode. Once derived CHEN5 was originally benchmarked against the GRI-Mech 2.11 detailed mechanism using both perfectly stirred reactors [41] and premixed flames [42]. CHEN5 predictions of temperature, CO (carbon monoxide), CH4 (methane) and NO (nitric oxide) showed agreements within 5% of the corresponding predictions coming from the full kinetic model for pressures between 1 and 30 atm and equivalence ratios ranging from 0.6 to 1.0. It is worth noticing that C2H2 (acetylene), which is usually considered as the main soot precursor [43], is not included among the CHEN5 mechanism transported species. Following this study objectives, the cost of using reduced mechanisms, in terms of computational time, constitutes a critical issue in the assessments performed here. Thus, even if CHEN5 does not allow transporting acetylene, this very small mechanism has been included here because it should yield a representative lower bound of the simulation time required by methane-air combustion processes. At the same time, the use of CHEN5 allows covering a wide range of reduced mechanism sizes, in terms of number of species and reaction steps, from smaller (CHEN5) to larger (ARM17) ones.

Table 1. Reduced chemical kinetic mechanisms studied.

Mechanism	Steps	Species	Based on	Source	Reference
CHEN5	5	9	GRI-Mech 2.11	User	[36,37]
CHEN12	12	16	GRI-Mech 2.11	Sandia	[27,38]
ARM2	15	19	GRI-Mech 2.11	Sandia	[38,39]
ARM12	12	16	GRI-Mech 3.0	Author	[28,40]
ARM13	13	17	GRI-Mech 3.0	Sandia	[38]
ARM15	15	19	GRI-Mech 3.0	Author	[28,40]
ARM17	17	21	GRI-Mech 3.0	Author	[28,40]

CHEN12 is the GRI-Mech 2.11-based version of the GRI-Mech 1.2-based mechanism [27], consisting of 16 species and 12 lumped reaction steps aiming to represent methane-air combustion processes. The reduced mechanism giving rise to CHEN12 constitutes one of the first efforts made in order to develop a mechanism providing a more comprehensive description of combustion phenomena than those early mechanisms involving four- to five-steps only. As part of the derivation of this reduced mechanism,

comparisons carried out include perfectly stirred reactor responses, auto ignition and shock-tube ignition delay times, laminar flame propagation speeds and ignition-extinction limits of counter flow flames. In general, for these combustion phenomena, good to excellent predicting performance has been reported [27], for a range of thermodynamical parametric variations, including those of temperature, pressure and composition. Pressures and equivalence ratios ranging from 0.25 to 20 atm and from 0.5 to 2.0, respectively, were originally considered for verifying the CHEN12 results. More specifically, some of these results indicate that, for pressures smaller than 1 atm, laminar flame speeds discrepancies (relative to the detailed mechanism) are within 4%, whereas for higher pressures, the CHEN12 performance improves significantly. Similarly, by considering counter flow nonpremixed flames, it is shown that flame extinction limits are well predicted (largest errors around 6%). Notice that the CHEN12 mechanism (also known as ARM1) has been successfully employed for performing transported PDF-based simulations of turbulent nonpremixed flames [34].

The 15-step ARM2 [39] mechanism is the corresponding CHEN12 one that includes NO (nitric oxide) chemistry in methane-air combustion. The ability of both CHEN12 (ARM1) and ARM2 mechanisms to represent local extinction, re-ignition and other chemical phenomena observed in nonpremixed piloted jet flames has been investigated in [39], through PDF-based simulations of the Sandia flames D, E and F [35]. These numerical simulations show that the two mechanisms yield results that are very similar to each other, with slightly worse agreement with the experimental data when compared to the detailed GRI-Mech 2.11 and 3.0 mechanisms. For flame D, for instance, the CHEN12 and ARM2 calculations of burning indexes based on CO show values 17% smaller than the corresponding measured ones.

The reduced mechanisms ARM12, ARM15 and ARM17 [28] constitute an extension of early efforts [27] to account for the latest GRI mechanism release, GRI-Mech 3.0, and the description of NOx (nitrogen oxides) formation. Due to space limitations in the original work, verification results presented in [28] are restricted to the ARM15 reduced mechanism only. Accordingly, in order to assess the ARM15 predicting capabilities for methane-air combustion, global and structural responses of various reference combustion systems – including perfectly stirred reactors, freely propagating flames and nonpremixed counter flow flames – have been obtained with this reduced mechanism and the GRI-Mech 3.0 detailed mechanism. Technological processes, such as oxy-fuel burning and NO reburning, have been also considered during the ARM15 performance evaluation. The results from the assessments carried out show that, in general, the ARM15 exhibits good to excellent predictive capabilities. It is seen in particular that perfectly stirred reactor-based NO mole fractions are accurately predicted over a wide range of residence times at 1 and 20 atm pressure. A similar NO behavior is observed in the case of freely propagating flames for equivalence ratios of 0.7, 1.0 and 1.4. NO reburning related results obtained from a homogeneous, continuous flow device (flow reactor) show that the NH3 (ammonia) mole fractions are over-predicted by the ARM15. Nevertheless the temporal evolution of NO and HCN (hydrogen cyanide) is well captured. The last reduced mechanism studied in this work is the ARM13 mechanism. The ARM13 is essentially the ARM12 mechanism without the H2 (hydrogen) pathway associated to HO2 (hydroperoxyl) and H2O2 (hydrogen peroxide), but with NO chemistry including the chemical species NO, HCN and NH3.

As highlighted in [43], methane oxidation in flames proceeds mainly through H (hydrogen) abstraction by H, O (oxygen), and OH (hydroxyl) radicals, i.e., CH4 + (H,O,OH) ⇌ CH3 + (H2,OH,H2O), producing the methyl radical (CH3), plus H2, OH and H2O (water). The methyl radical is in turn consumed mainly by reactions with both O atoms and HO2, leading to the formation of CH2O (formaldehyde). Further abstraction of CH2O by H and OH leads to the formyl radical (HCO), which decomposes to yield CO (carbon monoxide) and H, or undergoes H abstractions by H and O2. Once CO is formed, the reaction process continues according to one of most important reaction steps characterizing hydrocarbon oxidation, that is, CO + OH → CO2 + H. This last reaction is responsible almost exclusively for converting CO to CO2 (carbon dioxide) [43]. In rich mixtures, the relatively large amount of CH3 both enhances their recombination leading to the formation of C2 species, such as C2H6 (ethane) and C2H5 (ethyl radical), and yields C2H4 (ethylene) via its reaction with CH2 radicals. These C2 species either undergo further oxidation, or lead eventually to C2H2 formation, if they survive the oxygenated species attack.

The acetylene oxidation process does not necessarily require H abstractions to initiate. The reaction between C2H2 and O yields CH2 and HCCO (ketenyl) radicals, according to C2H2 + O → CH2 + CO and C2H2 + O → HCCO + H. The ketenyl radical reacts in turn with H atoms to produce the singlet methylene radical and CO. In fuel rich mixtures, acetylene may also combine with H atoms to produce C2H3 (vinyl), which can be quickly oxidized when oxygen is available, leading eventually to the formation of C1 radical species [43]. From this point forward, the acetylene combustion continues following the oxidation mechanisms for methane described above.

Among all seven reduced mechanisms analyzed, CHEN5 only does not include C2H2. CHEN12, which forms the basis for the ARM1 and ARM2 mechanisms, involves some lumped reaction steps where C2 species, namely C2H6, C2H4 and C2H2, are considered. Only two global steps, O2 + CH3 + CO + C2H4 ⇌ CH4 + CO2 + CH2O + 0.5C2H2 and O2 + 0.5C2H2 ⇌ H + CO2, account for the formation and oxidation of acetylene in the CHEN12 mechanism. Similarly, the ARM12 mechanism, upon which the ARM13, 15 and 17 mechanisms are built up, includes as C2 species C2H6, C2H4 and C2H2. The formation of these species and their subsequent oxidation is carried out according to C2H6 ⇌ C2H4 + H2, C2H4 + OH ⇌ CH3 + CO + H2 and C2H2 + O2 ⇌ 2CO + H2.

These highlighted steps emphasize the fact that, for example, none of the reduced mechanisms analyzed explicitly includes reactions describing, in fuel rich mixtures, the acetylene production with H atoms yielding the vinyl radical (C2H3) [43]. In addition, C2H3 production can be important as well in fuel rich conditions due to the H abstraction of ethylene by H and OH. It is noteworthy that the C2H4-related steps do not consider this aspect. Finally, three other steps, C2H3 + (H,O2) → C2H2 + (H2,HO2) and C2H3 + M ⇌ C2H2 + H + M (M, third body), relating the vinyl radical and acetylene, are not accounted for in any of the reduced mechanisms studied in this work. Accordingly, even if the predictive capabilities of such mechanisms may be questionable in fuel rich conditions, the largest computational burden is expected to come from the reaction steps already present. Further work will involve expanding such reduced mechanisms to account for extra soot precursor steps.

Notice that all reduced mechanisms considered here use *ad hoc* Chemkin compatible rate calculation routines for the computation of chemical species production rates. These routines have been provided by

the mechanisms' developers along with the reduced mechanisms in Chemkin format. The description of each of these rate routines associated with the reduced mechanisms is out of the scope of this work. The interested reader may follow the references given in Table 1 for the details of such routines, the description of the chemical species and reactions composing each of these reduced mechanisms, as well as the rationale behind their derivation.

Finally, it is important to emphasize that the reduced mechanisms analyzed in this work have not been derived for the specific purpose of studying soot formation processes – CHEN5 for instance has been focused on fuel lean conditions, where the amount of soot formed is insignificant. However, this does not necessarily imply that such mechanisms are unsuitable for the purpose of studying soot. Indeed, this is the one of the main reasons why the present work has been performed, i.e., to evaluate the suitability of the reduced mechanisms considered for describing soot formation. Moreover, some of the key soot formation-related species are not present in the reduced mechanisms considered, nor in the detailed mechanisms where they were derived from. For instance, C6H6 (benzene), the simplest polycyclic aromatic hydrocarbon (PAH), which is crucial in the exploration of the formation pathways of soot precursors and soot, is not present in any of the reduced mechanisms considered in this work. This drawback would prevent using these reduced mechanisms in conjunction with relatively complex soot formation models such as the one described in [44]. In addition, the predicting capabilities of the reduced mechanisms studied here, regarding other central chemical species participating in soot formation and oxidation processes, such as C2H2 (acetylene) and OH (hydroxyl), have not been previously analyzed. It is mandatory then to study the response of these reduced mechanisms under soot forming conditions in order to elucidate its feasibility of use for soot modelling in turbulent flames.

2.2. Chemical reactor-based configuration

When applying transported PDF methods to turbulent combustion modeling, chemical reaction-related terms appear in closed form, which is a significant advantage when compared to classical presumed PDF approaches [45,46]. Since there is an interest in using reduced kinetic mechanisms in transported PDF-based approaches, it is important to consider, for the assessment of these mechanisms, model configurations representative of the strong turbulence-chemistry interactions that may occur in practical combustion systems. Chemical reactors, and more specifically partially stirred reactors (PaSRs) [47,48], are thus utilized for the assessment of the different reduced mechanisms studied in this work.

In chemical reactors, the influence of turbulent mixing on chemical reactions is paramount. In continuous combustion, this interaction may be identified as two continuous flow mixing modes [49]. 'Stream mixing', which occurs between fuel and air streams and is required to achieve locally flammable mixture proportions; and 'backmixing', in which recirculating partially or wholly burned gases are mixed with fresh reactants to achieve sustained self-ignition without the aid of external energy sources. Stream mixing is usually represented by plug flow reactors and backmixing by stirred reactors. The perfectly stirred reactor (PSR) is a reactor in which backmixing ('mixing') is assumed to be infinitely fast, so that the exit stream is representative of the homogeneous reactor contents. This infinitely fast mixing hypothesis leads to a situation where the residence time is the only time scale competing with the chemical reactions characteristic time [28]. For adiabatic conditions then, the PSR properties should approach chemical

equilibrium for large residence times, whereas extinction occurs when the residence time is reduced such that chemical reactions can no longer be sustained.

Nevertheless, for the modelling of turbulent combustion systems, the PSR approach may not be adequate, because it does not allow for macro level composition and temperature inhomogeneities. This has led to the use of partially stirred reactor (PaSR) models [50,51], where variations in mixture properties may be described statistically, even though only the gross flow features at the reactor exit are modeled. In PaSR-based models, the infinitely fast mixing assumption is relaxed. Hence, an additional parameter controlling the molecular mixing process, i.e., the mixing time scale, is required in PaSRs, which allows studying systematically the effect of finite rate mixing on chemical kinetics. Accordingly, two different parameters, namely, (i) the ratio between residence and mixing times and (ii) the ratio between residence and chemical times, characterize PaSRs [47]. The former describes how far from PSR conditions the PaSR is, whereas the later describes the PaSR proximity with respect to equilibrium or extinction. In this work, the interaction by exchange with the mean (IEM) model [52], also known as the linear mean-square estimation (LMSE) model [53], is used as mixing model. From the perspective of turbulent combustion modeling using transported PDF-based hybrid Euler/Lagrange schemes, a PaSR could be seen as representing a single Eulerian grid cell containing Lagrangian particles describing the combustion process. Due to its simplicity then, a PaSR allows evaluating detailed and reduced chemical kinetic mechanisms without significant computational cost, since the detailed fluid dynamics behavior is not addressed.

2.3. Soot Formation Model

A part of this study focus on the reduced mechanisms influence upon the soot formed inside the PaSR, which is modeled here using the classical Brookes and Moss two-equations model [54,55],

$$\frac{dN}{dt} = 54N_A\left(\frac{X_{C_2H_2}P}{RT}\right)e^{-21100/T} - \left(\frac{24RT}{\rho_s N_A}\right)^{1/2}\left(\frac{6}{\rho_s\pi}MN^{11}\right)^{1/6}, \tag{1}$$

$$\frac{dM}{dt} = \left\{54M_P e^{-21100/T} + 11.7e^{-12100/T}\left[\pi N\left(\frac{6M}{\rho_s}\right)^2\right]^{1/3}\right\}\left(\frac{X_{C_2H_2}P}{RT}\right) - 4.2325\times10^{-3}\left(\frac{X_{OH}P}{RT}\right)\sqrt{T}\left[\pi N\left(\frac{6M}{\rho_s}\right)^2\right]^{1/3}. \tag{2}$$

As evidenced by Eqs. (1) and (2), this simple soot formation model involves the transport of two soot properties: (i) the soot particles number density (N), i.e., the number of soot particles per reactor unit volume; and (ii) the soot mass density (M), i.e., the soot mass per reactor unit volume. From this second parameter, and assuming a constant value for the soot density (ρ_s), i.e., the soot mass per soot unit volume, equal to 1800 kg/m^3 [56], the soot volume fraction (f_v), i.e., the volume of soot per reactor unit volume, is readily obtained,

$$f_v = \frac{M}{\rho_s}. \tag{3}$$

Notice that in Eqs. (1) and (2), N_A stands for the Avogadro's number, M_P is the molar mass of an incipient soot particle (144 g/mol), which is assumed to consist of 12 carbon atoms [54], X is the molar fraction, R is the universal gas constant, and P and T represent the gas mixture pressure and temperature, respectively.

Following the Brookes and Moss soot model, when computing the production rate of soot particles, both nucleation and coagulation of soot particles are considered, first and second right hand side (RHS) terms of Eq. (1), respectively. The soot mass concentration involves in turn the creation of soot mass by both particle nucleation (Eq. (2) first RHS term) and surface growth processes (Eq. (2) second RHS term). Finally, the soot oxidation is carried out according to Eq. (2) last RHS term. As it may also be seen from Eqs. (1) and (2), the concentrations of two key soot-related species, namely C2H2 and OH, explicitly appear in the Brookes and Moss soot model. More specifically, C2H2 is considered as a soot precursor and OH as a soot oxidizing species, and their concentrations act in these equations as linear source terms, whereas temperature controls the soot formation via an Arrhenius-type dependency. Accordingly, the accurate prediction of temperature, C2H2 and OH concentrations present inside the PaSR is crucial for determining the soot distribution. Indeed, even if stochastic fluctuations of C2H2 and OH within the PaSR are linearly coupled with the N and M evolution, a non linear behavior of the soot properties is expected to result, due to the power law dependency on N and M.

Following the modeling methodology described in Section 2 thus, results using the reduced mechanisms summarized in Table 1 have been obtained and compared with each other, as well as with those corresponding to the detailed GRI-Mech 2.11 and 3.0 mechanisms. The main outcomes from such comparisons are both described and discussed in Section 4.

3. Numerical Approach

In order to assess the performance of the reduced mechanisms described in Section 2.1, in terms of accuracy and computational time, several PaSR simulation results have been obtained in this work. The simulations have been performed considering two separate inlet streams, one involving pure methane as fuel, and the other involving air as oxidant, both at 300 K and 1 atm. For ensuring a swift ignition of the inflow streams, an atmosphere of pure CO2 (carbon dioxide), at 2100 K and 1 atm, has been used as initial composition inside the PaSR. All results have been obtained keeping constant the ratio of residence to mixing times, tres/tmix = 10. This value has been chosen such as to consider a fast mixing situation, but not so fast to avoid getting close to the PSR limit (tres/tmix $\rightarrow \infty$).

Two sets of results are discussed in sections 4.1-4.2 and 4.3. The first set relates to the assessment of the reduced mechanisms predictive capabilities, with and without chemistry acceleration techniques. Analyses of the predictions performed for various chemical species, including the key soot-related ones such as C2H2 and OH are carried out. A total number of notional particles (inside the PaSR) of 4000 is considered in all simulations, along with a constant residence time of 80 ms. The total simulated time (t) corresponds to 25 residence times, i.e., 2 s, as soot-related properties will be seen to take a relatively long time to achieve quasi-steady state conditions, when compared to temperature, for instance. Additionally, three different equivalences ratios, ϕ, obtained by changing the number of fuel particles entering the PaSR,

i.e., 1.10, 1.50 and 1.92, are studied. These fuel rich mixtures are chosen such as to simulate reactor conditions presenting a significant amount of soot. Higher mixture equivalence ratios lead to numerical simulations difficulties, regarding the attainment of reactor converged solutions, at least when using the reduced mechanisms studied here.

The computational burden associated with the use of the reduced mechanisms is also considered as a central aspect in this work. Accordingly, the first set of obtained results includes two parts, one involving the application of direct integration processes only (Section 4.1) and the other involving, additionally, a chemistry acceleration technique (Sections 4.2). A particular implementation of the *in situ* adaptive tabulation (ISAT) technique [57], which is used for reducing the amount of computer time required to treat chemistry in reactive flow calculations, is utilized here. Shortly, ISAT involves an adaptive tabulation of the composition space accessed region, where adaptation is used to control the tabulation errors. Speed-up factors of about 1000 are usually associated with ISAT when compared to the direct approach of numerically integrating the PaSR equations [57]. The specific details of the particular ISAT scheme used in this work can be found in [58]. In this work, when ISAT is used as a chemistry acceleration technique, an error tolerance of 10^{-5} is considered. The PaSR-related routines along with the ISAT technique compose the so-called ISAT@PaSR platform that is used here for computing the reduced mechanisms results.

The second set of results analyzed specifically focuses on soot properties (Section 4.3). These results have been obtained together with those discussed in Section 4.2, which involve the use of chemistry acceleration techniques. The same PaSR-based configuration and its associated initial and inlet conditions described above, along with the same equivalence ratios and residence time, have been therefore employed for obtaining this second set of results. Similarly, it implies that all results discussed in Section 4.3 have been obtained when chemistry acceleration techniques are used. Finally, it is worth highlighting that in this work all chemistry-related computations are treated using Chemkin II routines [59]. More specifically, reaction processes are modeled using Arrhenius laws and integrated using SUNDIALS/CVODE [60].

4. Results and Discussion

The results obtained from the different PaSR numerical simulations carried out in this work are discussed in this section. For the sake of clarity, the analysis and discussion of the results is divided into three sections. The first one (Section 4.1) involves direct integration-based results, the following (Section 4.2) relates to chemistry acceleration techniques based-results, and the final one (Section 4.3) focuses on soot-related results. All results have been obtained using an Intel® Xeon® Processor E5-2680 v0, 2.70 GHz and 128 GiB of RAM memory, along with Intel® C and Fortran (v. 13.1.1) compilers.

4.1. Direct integration-based results

This section discusses results obtained by direct integration of the Arrhenius laws describing the chemical reaction processes only, i.e., without resorting to any chemistry acceleration technique.

4.1.1. Temporal evolution

Figure 1 illustrates, for a mixture equivalence ratio of 1.92, the history, in terms of both means (top plots) and variances (bottom plots), of the reactor temperature, OH and C2H2 mass fractions, according to the two detailed mechanisms, GM211 and GM30, and the seven reduced mechanisms studied. In this work,

at any time step, the mean and variance of a given PaSR property, such as a species mass fraction Y, are computed as, respectively,

$$\langle Y \rangle = \frac{1}{n_p} \sum_{i=1}^{n_p} Y_i, \tag{4}$$

$$var(Y) = \frac{1}{n_p} \sum_{i=1}^{n_p} (Y_i - \langle Y \rangle)^2, \tag{5}$$

where n_p stands for the number of stochastic particles within the reactor. Notice that, for the sake of clarity, the curves characterizing a given mechanism have the same color (and marker) throughout the paper.

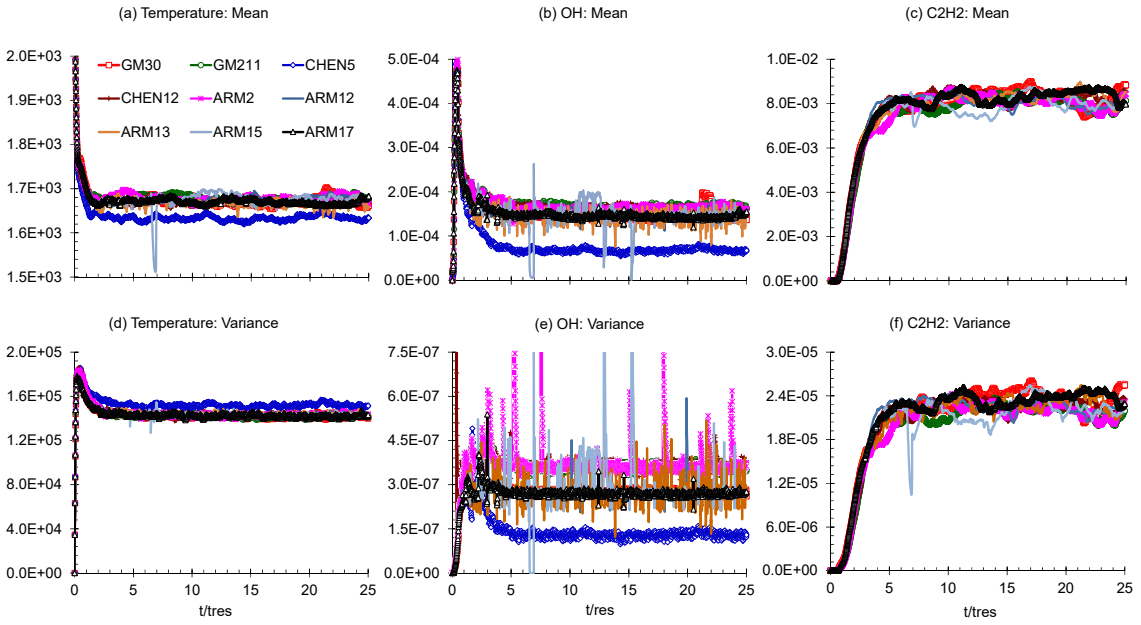

Figure 1. Temperature and OH and C2H2 mass fractions history (ϕ = 1.92) (top: mean, bottom: variance).

It is seen from Figure 1b that the OH reduced mechanisms results seem to follow the corresponding detailed mechanisms where they were derived from. Accordingly, mechanisms CHEN5, CHEN12 and ARM2 follow the GM211, whereas mechanisms ARM12 to ARM17 follow the GM30 detailed mechanism. This desired behavior is observed for both OH mean and OH variance values. Excepting the smallest reduced mechanism analyzed (CHEN5), similar trends characterize the temperature results (Figure 1a and d). Nevertheless, in this particular case, it is more difficult to distinguish the different reduced mechanism results from each other, as in the plots the results seem to mix altogether. The CHEN5 temperature trends could be considered as an exception to those ones corresponding to the other reduced mechanisms studied. It is believed that the relatively small number of chemical species and reaction steps characterizing this mechanism, which directly influence the heat release level is partially responsible for this particular behavior. Finally, no particular patterns characterize the C2H2 reduced mechanisms results (Figure 1c and f). Moreover, it is observed from the C2H2 plots that some large scale fluctuations remain even after 25 residence times. Since the computed C2H2 fluctuations are observed as well in the detailed mechanisms

results (GM211 and GM30), they could be associated with the existing knowledge of the C2H2 chemical reaction rates.

Figure 1 highlights as well that each chemical species has its own fluctuation frequency, i.e., its own chemical time scale. When compared to C2H2 for instance, OH present a smaller time scale. This implies in practice that OH takes less time steps than C2H2 to achieve a steady state. It is worth noticing that, as Figure 1c and f illustrate, the C2H2 steady state is indeed characterized by relatively large fluctuations, which remain even when time periods longer (100 residence times, for instance) than those considered in this work are simulated. Similarly, from Figure 1 it is observed that temperature has its own fluctuation frequency and its steady state value is achieved after about 5 residence times. Notice as well that, in terms of temperature, the final steady state values characterizing all reduced mechanisms, excepting CHEN5, show a good agreement with the value corresponding to the detailed mechanisms, i.e., the differences between the detailed and reduced mechanisms are of the order of 1%.

In terms of temperature and OH mass fraction, it has been observed that both CHEN12 and ARM2 closely follow the GM211 detailed mechanism. Similarly, ARM12 to ARM17 closely follow the GM30 corresponding one. It is believed that this occurs because what differentiates these reduced mechanisms (the description of NOx formation, essentially) has a small influence on both the heat release and the chemical species time scales. Figure 1 results indicate then that there is no need to consider all reduced mechanisms for further analyses. Selecting one representative reduced mechanism from each of the two groups, GM211- and GM30-related mechanisms, seems to be enough for what is intended in this work. Nevertheless, it is worth noticing that different computational times characterize each of the reduced mechanisms studied. For instance, it has been observed that in general the computational time associated with the ARM12, ARM13 and ARM15 mechanisms lie between those values corresponding to the CHEN5 and ARM17 mechanisms, which are discussed in the following sections. Accordingly, henceforth the analysis will be restricted to the first, third and last of the reduced mechanisms listed in Table 1, i.e., CHEN5, ARM2 and ARM17. These three reduced kinetic mechanisms are chosen for the analyses because they represent, respectively, the smallest mechanism considered, the mechanism that has been usually adopted for simulating turbulent flames, and the mechanism that involves the latest GRI-Mech release.

4.1.2. Mechanisms accuracy

The reduced mechanisms accuracy has been evaluated by analyzing steady state results of selected properties characterizing the PaSR. For the sake of simplicity, the end of the period simulated (2 s or 25 residence times) has been considered as representative of the reactor steady state condition. Properties considered for the analyses include the reactor temperature and the mass fractions associated with both minor – OH, C2H2 and CO – and major species – CH4 and O2. Accordingly, Figure 2 shows, as a function of the mixture equivalence ratio, the relative discrepancies (%) between the results corresponding to each of the reduced mechanisms considered and those associated with the GM211 and GM30 detailed mechanisms. Notice that, in accordance with their corresponding origin, CHEN5 and ARM2 are compared with GM211, whereas ARM17 is compared with GM30. More specifically, for a species mass fraction Y, for instance, the relative discrepancies are computed as follows,

$$\Delta Y_{red.mech} = \left(\frac{Y_{red.mech} - Y_{det.mech}}{Y_{det.mech}}\right) \times 100\%. \quad (6)$$

There are several points to highlight in Figure 2. It is observed for instance that the reduced mechanisms accuracy varies with the equivalence ratio. Since reduced mechanisms are usually derived for a set of particular conditions, this result is not surprising. More specifically, the discrepancies in the reduced mechanisms mixture temperature predictions increase with the increase in the equivalence ratio. The ARM2 and ARM17 temperature discrepancies remain however below 1.5%. Furthermore, from the three equivalence ratios analyzed, that roughly characterizing stoichiometric conditions (1.1) presents the best temperature predictions. Figure 2 shows as well that, except for OH and CO, the CHEN5 predictions accuracy is higher as equivalence ratio tends to stoichiometric conditions. This is something than could have been expected, as this mechanism has been specifically tailored for stoichiometric to fuel lean conditions. Notice however that in terms of OH and CO mass fractions, the best CHEN5 accuracy results are obtained for an equivalence ratio around 1.5. In addition, as the equivalence ratio increases, the discrepancies in the ARM2 predictions for OH decrease, whereas for C2H2 they initially increase and then decrease. Something similar occurs with the discrepancies in the ARM17 predictions for C2H2. However, the discrepancies in OH predictions associated with ARM17 first decrease and then increase as equivalence ratio increases.

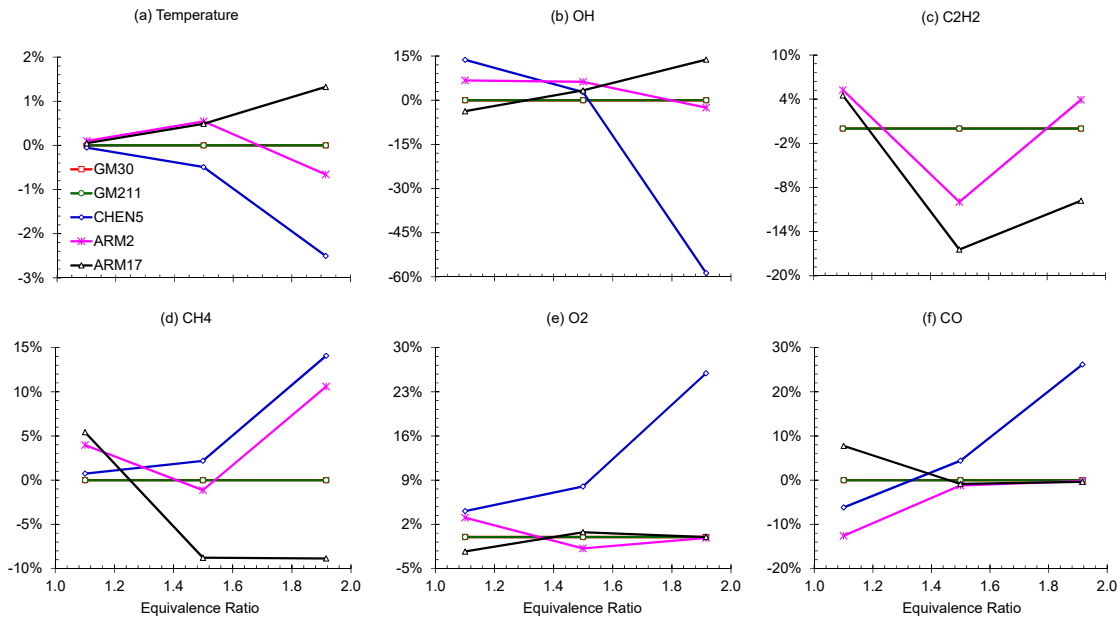

Figure 2. Reduced mechanisms discrepancies (%), in terms of temperature and selected species mass fractions, as a function of equivalence ratio (reference values used for computing relative discrepancies: GM211 and GM30 detailed mechanisms) – Direct integration.

It is also observed from Figure 2 that, in terms of accuracy, the worst reduced mechanisms predictions are obtained using CHEN5 at the highest equivalence ratio studied (1.92). This result can be associated to both (i) the fact that this reduced mechanism was developed with focus on conditions other than fuel rich ones, and (ii) the relatively small number of species and reaction steps characterizing this reduced mechanism. Increasing the number of chemical species and reaction steps characterizing a given mechanism implies adding more chemical pathways, which improve the chemical time predictions. When

carrying out such a process in a reduced mechanism, it is expected in general that the accuracy of its associated predictions increases as well. Nevertheless, the accuracy with which a given species is predicted will improve only if the added species and reaction steps directly or indirectly affect the species under consideration. ARM2 and ARM17 have a similar number of species and reaction steps for instance. The discrepancies in their associated predictions as a function of equivalence ratio vary however, as shown in Figure 2. At an equivalence ratio of 1.92, for instance, the ARM2 and ARM17 predictions for O2 and CO are essentially the same. Nevertheless, for the same equivalence ratio, significant differences appear in the CH4 and C2H2 discrepancies. The differences in the trends characterizing the Figure 2 ARM2 and ARM17 curves seem to come from several sources, including the species and reaction steps considered, as well as the chemical reaction rates that characterize each of the two detailed mechanisms (GM211 and GM30), from which these reduced mechanisms were derived.

In addition, Figure 2 illustrates that, for those species that are important in soot formation processes, i.e., OH (Figure 2b) and C2H2 (Figure 2c), the largest ARM2 discrepancies are of the order of 7% (OH) and 10% (C2H2), whereas the maximum ARM17 ones are about 14% (OH) and 16% (C2H2). The largest CHEN5 discrepancies for OH are in turn of the order of 59%. Notice that all maximum values for the discrepancies indicated here correspond to those fuel rich conditions where soot computations are relevant, i.e., equivalence ratio above ~1.5. The figures provided imply that, in principle, both ARM2 and ARM17 mechanisms could be utilized for soot formation studies without any restriction. Obviously, the same cannot be said for the CHEN5 mechanism, as this mechanism does not include C2H2 as one of its chemical species. Accordingly, depending on the reduced mechanism application, a mechanism size-related compromise needs to be achieved at some stage, so as to diminish the computer time involved, albeit preserving the prediction accuracy. Overall, the results shown in Figure 2 provide the order of magnitude of the errors that can be expected when using reduced mechanisms such as those considered here.

4.1.3. Computational time

The mechanism size, i.e., the number of chemical species and reactions, partially controls the time required to complete a given number of simulation time steps. In other words, the computational cost associated with the use of any chemical mechanism is directly related to the mechanism size. Nevertheless, the conditions in which the combustion process occurs, in terms of mixture equivalence ratio, for example, also influences the total cost that implies using a given kinetic mechanism. These aspects are emphasized in Figure 3, which shows the reduced mechanisms computational burden, expressed as a function of CPU (central processing unit) time, in both absolute (Figure 3a) and relative (Figure 3b) terms. More specifically, Figure 3b shows the relative computational cost characterizing each of the reduced mechanisms studied, which is computed using as reference the GM211 and GM30 detailed mechanisms, Eq. (7). Similar to the results shown in Section 4.1.2, in accordance with their origin, CHEN5 and ARM2 are compared here with GM211, whereas ARM17 is compared with GM30.

$$\Delta CPU_{red.mech} = \left(\frac{CPU_{red.mech} - CPU_{det.mech}}{CPU_{det.mech}}\right) \times 100\%. \quad (7)$$

Notice that the total CPU time, in absolute terms (seconds, s), shown in Figure 3a corresponds to the time required to complete 2000 time steps (25 residence times) of a PaSR-based simulation processing 4000

particles per time step. Accordingly, a gross estimate of the total time required by a typical hybrid Euler/Lagrange scheme-based simulation, involving 15 thousand time steps and 100 million particles, indicates that this time would be of the order of hundreds of years, i.e., 275 to 1510 years, approximately. These figures correspond to, respectively, the smallest reduced mechanism CHEN5 (equivalence ratio 1.92) and the detailed mechanism GM30 (equivalence ratio 1.1) utilized in this work. Even though parallel computing may reduce greatly these figures, these results emphasize both the large amount of computer time involved when performing transported PDF simulations, and the need of using chemistry acceleration techniques.

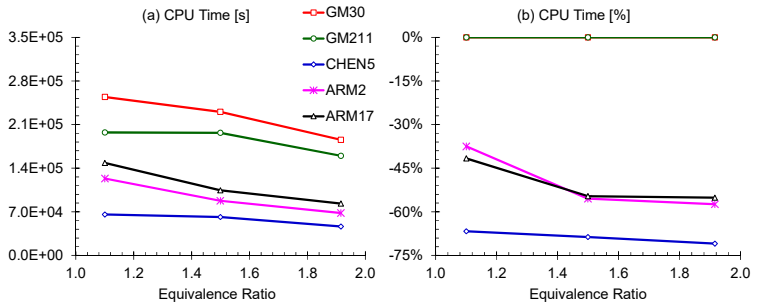

Figure 3. Detained and reduced mechanisms absolute (left) and relative (right) computational cost (reference values used for computing relative discrepancies: GM211 and GM30 detailed mechanisms) – Direct integration.

Figure 3 results also show that the computational cost associated with the use of kinetic mechanisms varies with the mixture equivalence ratio, and that, in general, this cost is the highest for stoichiometric conditions. This last outcome may be associated with the solution of the algebraic equations system, resulting from the integration of the Arrhenius laws describing the chemical reaction processes, which is possibly 'stiffer' at stoichiometric conditions. The referred stiffness may be a consequence of the particular dominant reaction mechanisms that prevail under these conditions. Additionally, as it could be expected, Figure 3 shows that the smallest reduced mechanism studied, CHEN5, presents the lowest computational cost. ARM17 features over 11% more species and over 13% more steps than ARM2. Figure 3a indicates in turn that ARM17 is in average 20% more costly than ARM2. It is generally accepted that the number of species plays a key role in the computational burden associated with a given mechanism, and that the number of reaction steps also influences this cost, although at a smaller degree. The results obtained here seems to confirm these aspects, but at the same time they seem to suggest that the existing interrelationship among the chemical species and reaction steps composing the kinetic mechanisms also contributes to the total cost that represent their usage. Notice as well from Figure 3a, that the ARM17 is the most costly among all studied reduced mechanisms.

Finally, Figure 3b emphasizes the fact that the savings in computational cost, because of the use of reduced mechanisms, may be significant. In particular, it is seen from this figure that the reduced mechanisms may lead to savings in computer time ranging from 38%, in the case of the ARM2 mechanism, to 71%, when the CHEN5 mechanism is considered. For equivalence ratios where soot formation is important, i.e., ~[1.5,1.92], and considering ARM2 and ARM17 only, the cost savings are of the order of 54% (ARM17) to 57% (ARM2). These large reductions in computational time are the main driving forces

for the development of reduced mechanisms and their use in numerical simulations involving practical combustion systems.

4.2. Chemistry acceleration technique based-results

The results discussed so far involved the application of direct integration processes only. In this section, the results obtained by using an ISAT-based chemistry acceleration technique [58] are discussed. When using an ISAT scheme, it may be useful to recreate the ISAT binary trees in the course of a computation. In simulations involving transient periods, for instance, binary tree recreations may help to discard the stored data, which may be seldom used during the statistical steady state part of the computation. The number of binary trees to be utilized in a given computation and their corresponding size need to be determined in a case-by-case basis.

A preliminary computer time-based analysis performed using the PaSR configuration utilized in this work showed that, in order to maximize the cost savings, the number of binary tree recreations should be kept as small as possible. The referred analysis suggested as well that small trees, in terms of memory size, should be preferred to larger ones. Accordingly, the ISAT-related results presented here have been obtained by using two binary trees only, with a single binary tree recreation always occurring at time step 800, i.e., after 10 residence times. In addition, a limit for the memory available for the binary trees of 150 MB has been imposed in all computations.

4.2.1. Mechanisms accuracy

Figure 4 shows, as a function of the mixture equivalence ratio, the results obtained using the particular ISAT scheme employed. In order to allow a fair comparison of the reduced mechanisms analyzed when using ISAT, the relative results illustrated in Figure 4 are computed using as reference the corresponding direct integration values. In other words, Figure 4 shows, for each mechanism, the relative discrepancies (%) between the results obtained using the ISAT-based technique utilized and those obtained through the use of direct integration (DI) only; i.e., for a species mass fraction Y, for instance,

$$\Delta Y_{mech} = \left(\frac{Y_{mech\_ISAT} - Y_{mech\_DI}}{Y_{mech\_DI}} \right) \times 100\%. \quad (8)$$

The properties shown in Figure 4 are identical to those given in Figure 2, i.e., temperature and OH, C2H2, CH4, O2 and CO mass fractions. Figure 4 results highlight that, for all properties, excepting CH4, the ARM17 ISAT usage discrepancies are found to be smaller than the ARM17 corresponding ones related to the case in which direct integration only is utilized (Figure 2). A similar scenario characterizes the ARM2 reduced mechanism. However, in this case, the exception is constituted by both temperature and OH mass fraction. It is particularly observed as well that the accuracy with which temperature is computed is relatively large, as the ISAT usage-related discrepancies are smaller than 1.1% (Figure 4a). For OH (Figure 4b) and C2H2 (Figure 4c), and considering only equivalence ratios where soot formation is important (above ~1.5), the maximum reduced mechanisms-related discrepancies are of order of 7% (ARM2) and 6% (ARM17), respectively. It is also interesting to note in Figure 4 that different discrepancy levels characterize the two detailed mechanisms analyzed. Accordingly, the largest discrepancy associated with the use of ISAT, which is of the order of 21% (Figure 4c), is obtained with the GM211 detailed mechanism. Without considering the detailed mechanisms, CHEN5 presents the largest discrepancy associated with the use of

ISAT, 17% (Figure 4f). From those two reduced mechanisms that could be readily used with the soot model utilized in this work, and for equivalence ratios above ~1.5, the ARM2 one present the largest discrepancy, 9% (Figure 4d). Additionally, for some properties such as O2 (Figure 4e) and CO (Figure 4f), the ISAT usage-related discrepancies associated with most of the mechanisms are observed to decrease as equivalence ratio increases. Nevertheless, in the case of temperature (Figure 4a), the opposite is found to occur. This means that for most of mechanisms studied here increasing the equivalence ratio leads to an increase in the temperature-related discrepancies.

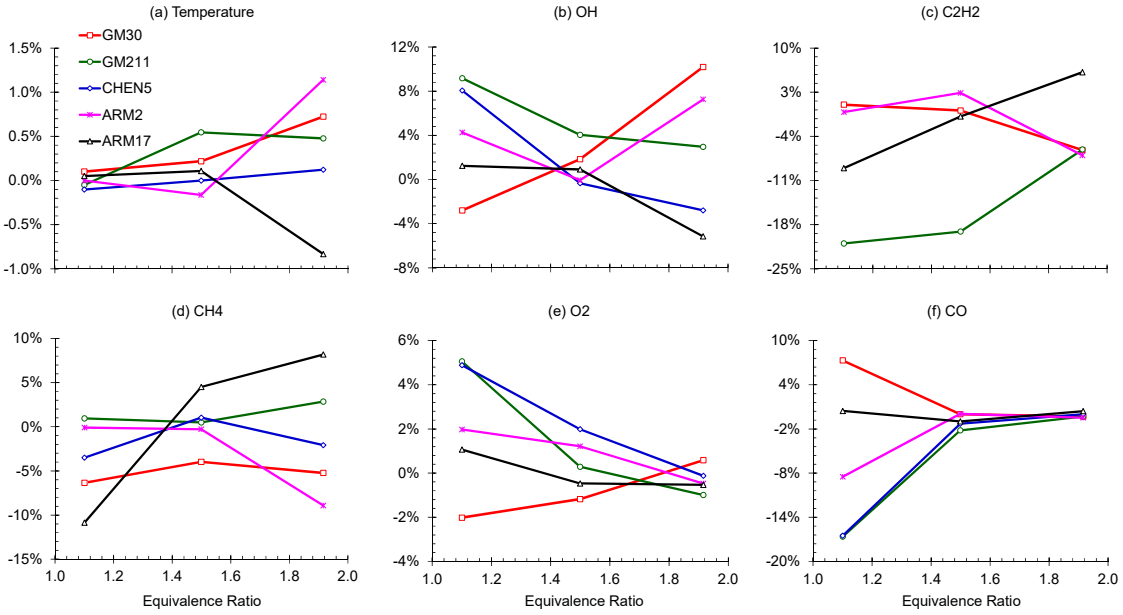

Figure 4. Detailed and reduced mechanisms discrepancies (%), in terms of temperature and selected species mass fractions, as a function of equivalence ratio (reference values used for computing relative discrepancies: direct integration-based results) – ISAT.

Finally, it is worth highlighting that, since the amount of computational time saved when using ISAT-related techniques may be substantial, as will be shown below, the ISAT findings discussed here are crucial. Notice also that the discrepancies reported in Figure 4 could be diminished by reducing the ISAT error tolerance, which was kept constant and equal to 10^{-5} in this work. Nevertheless, reducing this ISAT tolerance would bring penalties to the ISAT-related computational time savings. Once again, a compromise between accuracy and computational cost needs to be achieved at some stage. In this work no attempt to modify the ISAT error tolerance has been performed.

4.2.2. Computational time

Similar to what is presented in Figure 3 above, Figure 5 shows the time required, in both absolute (Figure 5a) and relative (Figure 5b) terms, to complete 25 residence times of the PaSR-based simulations carried out in this work using ISAT. More specifically, the relative results illustrated in Figure 5b are computed using as reference the corresponding direct integration values, i.e.,

$$\Delta CPU_{mech} = \left(\frac{CPU_{mech\_ISAT} - CPU_{mech\_DI}}{CPU_{mech\_DI}} \right) \times 100\%. \quad (9)$$

In absolute terms, Figure 5 shows that, for equivalence ratios below ~1.5, the computational cost trends observed when using ISAT are similar – in the sense that they remain practically constant or decrease with the increase in equivalence ratio – to those obtained without using any chemistry acceleration technique (Figure 3). Nevertheless, for equivalence ratios above ~1.5, the ISAT-related results present a completely different behavior. More specifically, it is observed that, excepting the reduced mechanism that does not allow computing soot formation (CHEN5), the CPU time absolute values associated with the other mechanisms increase with the increase of the equivalence ratio. This has been found to be a direct consequence of the particular soot model utilized in this work. In order to confirm this aspect, similar computations have been performed considering that the soot model features zeroed soot source terms, i.e., Eq. (1) and (2) RHS terms equal to zero. The results from this second group of computations are given in Figure 6. As it could have been expected, for equivalence ratios where soot formation is relevant (above ~1.5), all mechanisms CPU times (Figure 6a) follow this time the same trends obtained for the case involving direct integration processes only (Figure 3), which confirms the referred soot model influence mentioned above.

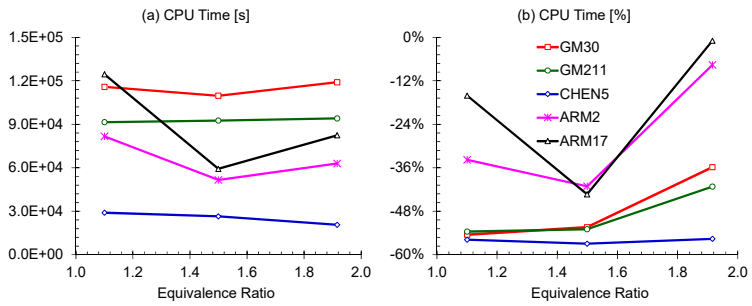

Figure 5. Detailed and reduced mechanisms absolute (left) and relative (right) computational cost (reference values used for computing relative discrepancies: direct integration-based results) – ISAT.

It may be noticed from Figure 5b that, for an equivalence ratio of 1.5, the relative costs reductions are considerable (41% to 57%). However, by comparing Figure 5b and Figure 6b, it is possible to observe that, for ϕ = 1.92, accounting for soot formation completely obliterates the computational time gains, which could be obtained with ISAT when chemistry is considered only. Indeed, the relative cost savings characterizing some of the reduced mechanisms are almost insignificant (~1% for ARM17), if the soot model is utilized. The decrement in the relative cost savings as soot formation becomes relevant comes from the difficulties that the soot model introduces in the ISAT tabulation process. More specifically, when computing the gradient of the reaction mapping [57], which is utilized in the linear approximation that ISAT carries out, singularities may appear at the fresh unburnt gases, i.e., when soot is absent (N, M $\rightarrow$ 0), but propensity for soot exists, [C2H2] > 0. These singularities are related to the particular soot model formulation used here. The use of this model leads indeed to mapping gradient matrix elements that are proportional to $N^{-2/3}$ and $M^{-5/6}$. Such a particular behavior is a reminiscence of the soot model derivation, which is not based on elementary chemical processes, but on curve fitting of experimental data. As a consequence, it seems that is not advisable to combine ISAT with empirically-derived soot models such as the present one.

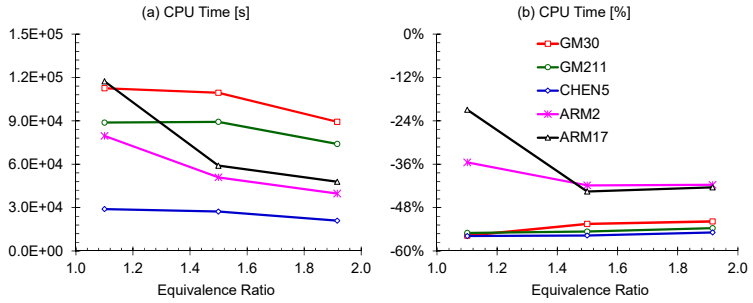

Figure 6. Detailed and reduced mechanisms absolute (left) and relative (right) computational cost (reference values used for computing relative discrepancies: direct integration-based results) – ISAT and soot model without soot source terms, Eq. (1) and (2) RHS terms equal to zero.

Furthermore, in a smaller degree, the soot model utilized seems to influence the reduced mechanisms ISAT-related results at an equivalence ratio of 1.1 as well. This aspect may be verified by comparing Figure 5b and Figure 6b, which show that, by zeroing the soot model source terms, the cost savings for ARM2 and ARM17 increase from 34 to 36%, and from 16 to 21%, respectively. It seems however that, at the equivalence ratio closer to stoichiometric conditions, what prevails is the chemical reaction mechanisms. Finally, for the two reduced mechanisms that allow computing soot, ARM2 and ARM17, and considering equivalence ratios above ~1.5 only, the ISAT-related time savings range from 8 to 41% and from 1 to 43%, respectively.

4.3. Soot-related results

As reflected in the classical Brookes and Moss soot model formulation, Eqs. (1)-(2), the accurate prediction of the minor chemical species and radicals that are responsible for soot formation and oxidation are crucial for determining the amount of soot formed. This is one of the reasons why C2H2 and OH, which actively participate in soot production processes, have been considered in the analyses of the reduced mechanisms carried out in Sections 4.1 and 4.2. In order to complement these analyzes, particular soot-related results are presented and discussed in this section. Notice that all results discussed in this section have been obtained simultaneously to those discussed in Section 4.2, and thus they involve the use of chemistry acceleration techniques.

4.3.1. Temperature, acetylene and hydroxyl accuracy

Before discussing specific soot results, it is important to illustrate the behavior of the three main properties, i.e., temperature, OH and C2H2 concentrations, influencing the soot model utilized (Section 2.3). Accordingly, Figure 7 shows the temporal evolution of the mean values of these three parameters, for an equivalence ratio equal to 1.92, obtained using the GM211 and GM30 detailed mechanisms, and the reduced mechanisms discussed in Section 4.2. Notice however that results corresponding to the CHEN5 reduced mechanism are not included in this section, as this mechanism does not allow for transporting the C2H2 concentration. Similar to what has been observed in Figure 1b, the OH reduced mechanisms results obtained using ISAT (Figure 7b) seem to follow the detailed mechanisms from which they were derived. Accordingly, the ARM2 reduced mechanism follows the GM211, whereas the ARM17 follows the GM30 detailed mechanism. Similar trends seem to characterize the temperature results (Figure 7a). However, in this case, the differences among the detailed and reduced mechanisms results are less noticeable. Notice as well that, as it happens in the case involving direct integration processes only (Figure 1c), the C2H2 ISAT-

related results obtained (Figure 7c) do not follow any particular pattern. Figure 7c indicates indeed that some large scale fluctuations remain even after 25 residence times for both detailed and reduced mechanisms.

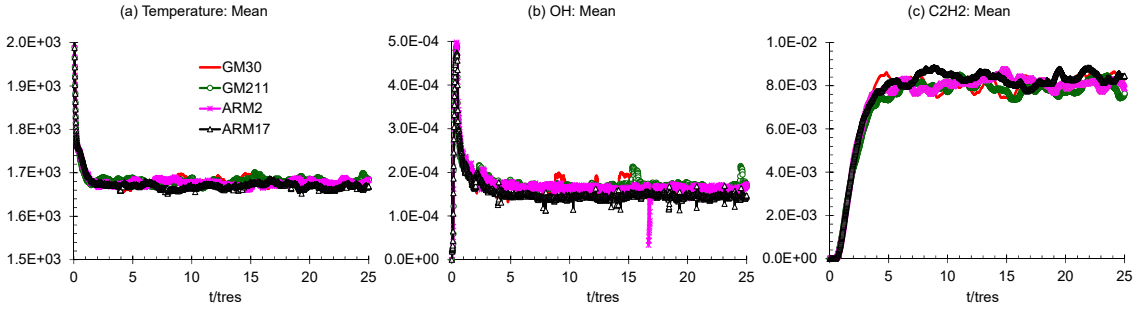

Figure 7. Temperature and OH and C2H2 mass fractions history (ϕ = 1.92) – ISAT.

From Figure 7 is possible to see that, while the mean values of temperature (Figure 7a) and OH mass fraction (Figure 7b) seem to somehow stabilize after 5 residence times, variations in C2H2 mass fraction mean values remain within the PaSR. Accordingly, as both it could be expected from Eqs. (1)-(2) and it will be seen below, the particular C2H2 behavior observed in Figure 7c is somehow reflected in the soot formed. It is important to emphasize at this point that, in terms of internal homogeneity, there are significant differences between perfectly and partially stirred reactors. A PSR is characterized by a homogenous composition and temperature, whereas a PaSR is a non-homogeneous system featuring a variety of internal compositions and temperatures, each of them corresponding to a given fluid (or notional) particle. In addition, in a PaSR, mixing between hot and cold (unburnt) gases, which occurs at a finite rate, plays a key role in the combustion process. Indeed, while some particles may react at high temperatures, others could undergo low temperature reaction processes. Accordingly, the dominant reaction mechanisms may vary substantially depending on the local (particle) thermodynamic states characterizing the combustion process. Therefore, the mean values of temperature, OH and C2H2 mass fractions appearing in Figure 7 are the result of averaging the fluid particles within the PaSR, Eq. (4).

Figure 8 top plots show the mean values of temperature, OH and C2H2 mass fractions computed using ISAT, characterizing the PaSR statistical steady state behavior, i.e., at the end of simulated period, as a function of the mixture equivalence ratio. Figure 8 bottom plots present in turn relative discrepancies (%) between the ISAT-related results computed for each of the reduced mechanisms considered and those direct integration processes-based ones associated with the GM211 and GM30 detailed mechanisms. More specifically, following their origin, ARM2 is compared with GM211, whereas ARM17 is compared with GM30. Thus, for a species mass fraction Y, for instance, the referred relative discrepancies are computed as follows,

$$\Delta Y_{mech} = \left(\frac{Y_{red.mech\_ISAT} - Y_{det.mech\_DI}}{Y_{det.mech\_DI}} \right) \times 100\%. \qquad (10)$$

Accordingly, the relative discrepancies appearing Figure 8, and in Figure 10 as well, give an order of magnitude of the total error that could be incurred because of the use of both reduced mechanisms and chemistry acceleration techniques.

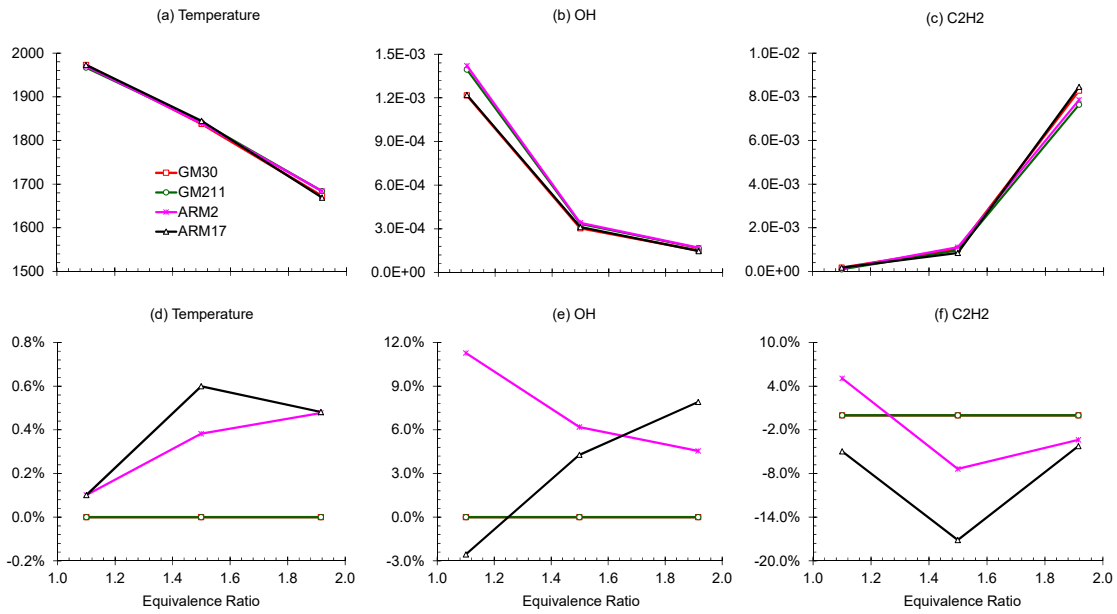

Figure 8. PaSR properties (top plots) and reduced mechanisms discrepancies (%) (bottom plots) as a function of equivalence ratio (reference values for computing relative discrepancies: GM211 and GM30 direct integration-based results).

It may be firstly noticed in Figure 8 that the temperature value (Figure 8a) characterizing the smallest equivalence ratio studied (1.10), ~1970 K, is lower than the corresponding adiabatic flame temperature (~ 2226 K). This is a direct consequence of the mixing process, which plays a key role in the PaSR-based configuration considered here [47]. In addition, in terms of temperature, it is seen that the accuracy of the reduced mechanisms could be considered as very good, since the discrepancies are smaller than 0.6% (Figure 8d). Additionally, in accordance with what may be observed from the OH temporal evolution (Figure 7b), the OH reduced mechanisms results seem to follow those corresponding to the detailed mechanisms considered. The ARM2 follows then the GM211 and the ARM17 follows in turn the GM30. Even when some remaining fluctuations are observed in the C2H2 temporal evolution (Figure 7c), it seems that the C2H2 reduced mechanism trends, as a function of equivalence ratio (Figure 8c), have a similar behavior as the OH ones do, i.e., they seem to follow the corresponding detailed mechanisms from which they were derived. Finally, for those equivalence ratios featuring significant amounts of soot (above ~1.5), the ARM2 discrepancies for OH range from 4 to 6%, and for C2H2 from 3 to 7%. Similarly, the ARM17 discrepancies are of the order of 4 to 8% for OH, and about 4 to 17% for C2H2. In average then, the ARM17 discrepancies for equivalence ratios above ~1.5 are larger than the ARM2 corresponding ones.

4.3.2. Soot particles number density and soot volume fraction accuracy

Concerning the soot properties results obtained, Figure 9 shows the history of the soot particles number density and soot volume fraction mean values, for an equivalence ratio of 1.92, according to the GM211 and GM30 detailed mechanisms and the two reduced mechanisms under consideration, ARM2 and ARM17. In terms of soot particles number density (Figure 9a), it may be observed that, after the initial transient, the reduced mechanisms-related results follow those corresponding to the detailed mechanisms from which they were derived. This means that the ARM2 follows the GM211 detailed mechanism, whereas the ARM17 mechanism follows the GM30 one. As it can be observed from Figure 9b, the same cannot be

affirmed in the case of the soot volume fraction. After the initial transient, the fv histories seem to follow different patterns, each of them featuring different fluctuation levels. The fluctuations characterizing the fv curves appear to be related to those associated with the C2H2 mass fraction (Figure 7c). The chemical species participating in the soot model utilized in this work (OH and C2H2) are certainly partially responsible for the particular trends observed in the soot curves. For the sake of argument, the discussion on the dynamic behavior characterizing the soot properties shown in Figure 9 will be postponed to Section 4.3.3 below.

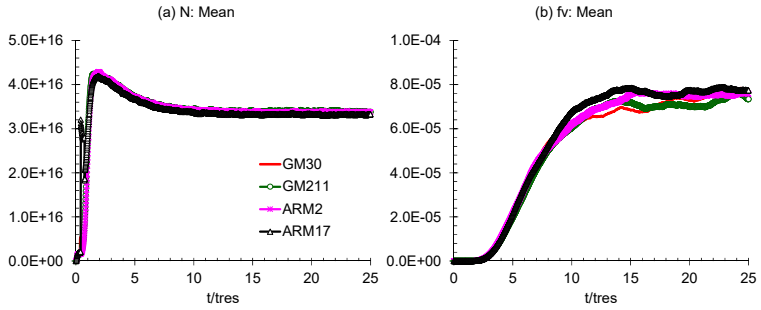

Figure 9. Soot particles number density (N) and soot volume fraction (fv) history (ϕ = 1.92) (N: 1/m^3, fv: m^{3}soot/m^3).

Figure 10 shows the soot formed (top plots) and the reduced mechanisms discrepancies (bottom plots), in terms of N and fv, as a function of the mixture equivalence ratio. These ISAT-computed N and fv values correspond to the mean values characterizing the PaSR at the end of the simulated period, i.e., 25 residence times. As before, the kinetic mechanisms discrepancies are computed according to Eq. (10). Unsurprisingly, Figure 10 top right plot highlights that the soot volume fraction increases sharply, from approximately 7.10^{-9} (ϕ = 1.1, ARM17) to 8.10^{-5} (ϕ = 1.92), with the increase in the equivalence ratio. This particular fv behavior with equivalence ratio could have been expected from the three properties that appear in Eq. (2), i.e., temperature, C2H2 and OH molar fractions, which in turn determine the fv values according to Eq. (3). Indeed, as shown in Figure 8a to c, for the ARM17 reduced mechanism for instance, with the increase in equivalence ratio, (i) temperature decreases (from 1970 to 1670 K), (ii) the soot precursor species C2H2 increases (from 2.10^{-4} to 9.10^{-3}), and (iii) the soot oxidizing species OH decreases (from 1.10^{-3} to 2.10^{-4}).

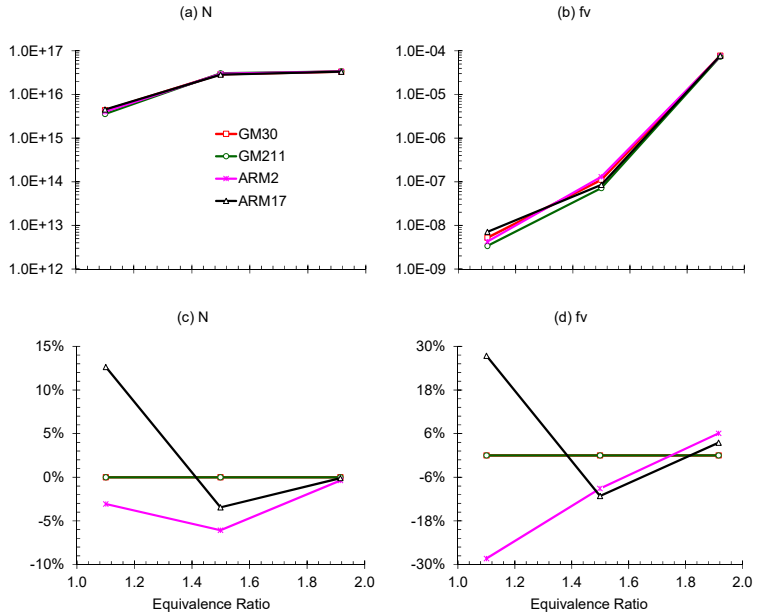

Figure 10. Soot production (N and fv) (top plots) and reduced mechanisms discrepancies (%) (bottom plots) as a function of equivalence ratio (reference values used for computing relative discrepancies: GM211 and GM30 direct integration-based results) (N: $1/m^3$, fv: m^3soot/m^3).

Similarly, Figure 10 top left plot shows that N also exhibits a monotonic evolution with the equivalence ratio. However, the steepness of the curves characterizing the N trends decreases as equivalence ratio increases. This particular behavior could be associated with the soot particles coagulation process occurring during soot formation. Indeed, as may be seen by examining Eq. (1) RHS second term, the larger the number of soot particles and the larger their mass, the more enhanced is the soot particles coagulation process. As a result, even though N initially increases with equivalence ratio, due to the increase in C2H2, from about 4.10^{+15} (ϕ = 1.1) to 3.10^{+16} (ϕ = 1.50), it then increases less steeply with further increases in equivalence ratio, reaching 4.10^{+16} (ϕ = 1.92). In addition, similar to what has been observed when discussing the chemical species present in the gas mixture (Figure 2, Figure 4, and Figure 8), Figure 10 bottom plots show that the discrepancies of the soot predictions performed using the reduced mechanisms vary with equivalence ratio. Notice that the largest fv discrepancies, obtained for ϕ = 1.1, could be considered as unphysical, as fv tends to zero at this condition (Figure 10 top right plot). For equivalence ratios in the range [1.50-1.92], the maximum reduced mechanisms fv discrepancies are of the order of 11 (AMR17) and 6% (ARM2) for ϕ = 1.50 and 1.92, respectively. The maximum N discrepancies computed, which range from 6 (ARM2) to 0.4% (ARM2) for $\phi \in$ [1.50-1.92], are in turn smaller than those associated with fv. It is worth emphasizing that is important to predict properly the amount of soot-related chemical species, such as OH and C2H2, as they will affect the accuracy of the corresponding soot predictions. The findings discussed here underscore overall the need of accurately predicting minor chemical species and radicals if soot predictions are to be effected.

Regarding the reduced mechanisms predicting accuracy specifically, Figure 10b bottom plots show that, for equivalence ratios where soot formation is relevant (above ~1.50), the ARM17 reduced mechanism present the smallest discrepancies in terms of N. The same occurs in the case of fv for an equivalence ratio of 1.92. The ARM2 reduced mechanism exhibits in turn smaller fv discrepancies than the ARM17 one, for

an equivalence ratio of 1.50. Notice that all reduced mechanisms present fv discrepancies of the order of 11% or less for equivalence ratios above ~1.5. Considering the uncertainty values that usually are associated with measuring fv [55], the discrepancy obtained could be considered as good enough for the purpose of simulating turbulent flames. Thus, reduced mechanisms presenting good temperature and (soot-related) species concentrations predicting accuracy, for equivalence ratios above ~1.5, seem to be enough for what is intended in terms of soot determination. All reduced mechanisms analyzed in this section present such good predicting accuracy, so they are expected to yield reasonable results when utilized for describing the soot formation in combustion systems.

4.3.3. Further discussion on soot properties dynamic behavior

Coming back to the temporal evolution of N and fv shown in Figure 9, it may be observed from the mean values characterizing these soot properties that, beyond 10 residence times, N (Figure 9a) practically remains constant, i.e., noticeable N variations are not observed anymore. Contrarily, fv (Figure 9b) exhibits a distinct behavior to that associated with N. Specifically, it is seen that fv varies even after 10 residence times, and some fluctuations in the fv values appear. These fv fluctuations may be associated with those ones characterizing the C2H2 curves (Figure 7c), although it seems that the dynamic response of the former is slower than that of the latter ones. Indeed, it is hard to affirm that the particular N and fv trends shown in Figure 9 directly correlate with either temperature, OH or C2H2 (Figure 7), as the trends in the soot properties come from the coupling of complex processes involving nucleation, coagulation, surface growth and oxidation of soot particles. Notice that all these soot formation-related processes are represented in the particular soot model utilized, Eqs. (1)-(2).

The long term (low frequency) fv fluctuations observed in Figure 9b may be a reminiscence of soot presence related intermittency, which has been reported in literature [61]. Notice that, in this context, intermittency regards to soot presence, which in turn involves both the number of soot particles and the soot mass, i.e., N and M (or fv). When soot intermittency is present then, in principle, both N and M (or fv) parameters are expected to be characterized by an intermittent behavior. However, as it may be seen in the results shown in Figure 9a, it seems that N does not exhibit such a behavior. Examining in detail this intermittent behavior is outside the scope of the present work.

5. Conclusions

In this work seven reduced chemical kinetic mechanisms utilized for methane-air combustion have been assessed. The reduced mechanisms evaluated involved different levels of complexity, in terms of numbers of chemical species and reaction steps. The assessment was carried out using partially stirred reactors, with and without ISAT-based chemistry acceleration techniques, by comparing the results obtained with those corresponding to detailed chemical kinetics baseline computations.

In terms of accuracy, for equivalence ratios where the amount of soot formed is significant, i.e., $\phi >$ ~1.5, and considering only those mechanisms that are readily used with the soot model utilized here, the reduced mechanisms results showed that major species are in general predicted reasonably well (~0-10% discrepancies). Nevertheless, larger discrepancies between detailed and reduced mechanisms results (~0.2-16%) were observed when predicting minor species. The ISAT technique used in this work led to further

reductions in the accuracy of the minor species predicted, i.e., to further increases in discrepancies (~0.1-7%). Regarding the computational cost, the results showed that savings of up to 57% can be obtained when using the reduced mechanisms analyzed. The use of ISAT techniques resulted in further cost reductions ranging from 1 to 43%. Discrepancies in the predictions of soot volume fraction of the order of 4-11% were observed when using reduced mechanisms.

From the results obtained in this work it is concluded that, even though they may lead to significant reductions in computational time, both reduced kinetic mechanisms and chemistry acceleration techniques may affect the accuracy of the obtained results. This is particularly true when minor species are accounted for. Overall, the results discussed here emphasize the need of both (i) carefully selecting the reduced mechanism that is more suitable for a given application, and (ii) adequately setting the chemistry acceleration technique to be utilized in the simulation process. From the results of the two methane-air reduced mechanisms analyzed in a soot formation context, the ARM17 mechanism could be recommended for simulating sooting flames. This recommendation is based on the fact this mechanism both (i) leads more often to the smallest discrepancies, in terms of soot particles number density and soot volume fraction, for equivalence ratios above ~1.5, and (ii) involves the latest GRI Mech release. Further work will involve using this reduced mechanism in contexts involving hybrid Euler/Lagrange approaches [10,11] that allow modeling practical combustion systems. For recommendations about the ISAT settings, see the Appendix section.

Finally, it is worth emphasizing that comparisons of numerical and experimental soot results require a proper numerical estimation of the soot volume fraction, as this parameter is usually the measured one. The results obtained in this work highlight that, even after a relatively large number of residence times, soot volume fraction low frequency fluctuations remain. This occurs when using both reduced and detailed kinetic mechanisms. The referred soot volume fraction fluctuations may have their origin in the corresponding C2H2 ones, which also remain, even for the detailed chemical kinetic mechanisms. This particular C2H2 behavior is clearly an outcome of the existing knowledge of the chemical reaction rates leading to C2H2. Assessing the validity of the computational results obtained should require the development of specific experimental studies. The findings from this work seem to suggest then that the main difficulties faced when comparing experimental and numerical soot volume fraction results should not come from the kinetic mechanism, but from the way in which the physics involving the soot formation is described. This would shift of course the concern from the kinetic mechanisms to the soot formation models employed.

6. Acknowledgments

This work was supported by Petrobras under the technical monitoring of Dr. Ricardo Serfaty (Project: Development of a modeling technique for turbulent combustion based on an Eulerian/Lagrangian approach – Phase II, Contract No.: 0050.0080122.12.9). During this work Luís Fernando Figueira da Silva was on leave from the Institut Pprime (CNRS - Centre National de la Recherche Scientifique, France).

7. Appendix

Regarding the recommended settings for the ISAT-based chemistry acceleration technique utilized in this work, there are several aspects to be considered, including (i) the ISAT error tolerance, (ii) the number of binary trees used to tabulate the composition space accessed region, and (iii) the amount of memory allocated for storing the tabulated data. Increasing the ISAT error tolerance implies not only obtaining more cost savings, but also introducing larger errors associated with the linear extrapolation that is part of the ISAT approximation. Acceptable values for this error tolerance were found to be of order of 10^{-6} to 10^{-3}. When accuracy is a critical issue, the tightest tolerances are preferred, which in turn penalize the computational cost. In simulations involving transient periods, such as those carried out in this work, it is important to recreate the ISAT binary trees, as this allows discarding stored data that may be seldom used during the statistical steady state part of the computation. The number of binary trees to be utilized, i.e., the number of binary tree recreations, and the corresponding size, needs to be determined in a case-by-case basis. Accordingly, the simulations performed have shown that the best results, in terms of cost savings, are obtained using two binary trees only, with binary tree recreation occurring between 5 and 10 residence times. The results obtained have shown as well that small trees (~150 MB, in memory size) are preferred to larger ones. These figures are expected to change of course when dealing with different physical problems. Nevertheless, they should provide a general idea of what could be expected when employing ISAT-based chemistry acceleration techniques, as those utilized in this work.

8. References

1. Pope, S, 1985, "PDF methods for turbulent reactive flows", *Progress in Energy and Combustion Science*, Vol. 11, pp. 119-192.
2. Haworth, D.C., 2010, "Progress in probability density function methods for turbulent reacting flows", *Progress in Energy and Combustion Science*, Vol. 36, pp. 168-259.
3. Jenny, P., Pope, S.B., Muradoglu, M. and Caughey, D.A, 2001, "A hybrid algorithm for the joint PDF equation of turbulent reactive flows", *Journal of Computational Physics*, Vol. 166, pp. 218-252.
4. Muradoglu, M., Liu, K. and Pope, S.B., 2003, "PDF modeling of a bluff-body stabilized turbulent flame", *Combustion and Flame*, Vol. 132, pp. 115-137.
5. Raman, V., Fox, R.O. and Harvey, A.D., 2004, "Hybrid finite-volume/transported PDF simulations of a partially premixed methane–air flame", *Combustion and Flame*, Vol. 136, pp. 327-350.
6. Raman, V., Pitsch, H. and Fox, R.O., 2005, "Hybrid large-eddy simulation/lagrangian filtered-density-function approach for simulating turbulent combustion", *Combustion and Flame*, Vol. 143, pp. 56-78.
7. Andrade, F.O., Figueira da Silva, L.F. and Mura, A., 2011, "Large eddy simulation of turbulent premixed combustion at moderate Damköhler numbers stabilized in a high-speed flow", *Combustion Science and Technology*, Vol. 183, pp. 645-664.
8. Vedovoto, J.M., da Silveira Neto, A., Mura, A. and Figueira da Silva, L.F., 2011, "Application of the method of manufactured solutions to the verification of a pressure-based finite-volume numerical scheme", *Computers & Fluids*, Vol. 51, pp. 85–99.
9. Yang, Y., Wang, H., Pope, S.B. and Chen, J.H., 2013, "Large-eddy simulation/probability density function modeling of a non-premixed CO/H2 temporally evolving jet flame", *Proceedings of the Combustion Institute*, Vol. 34, pp. 1241-1249.
10. Vedovoto, J.M., da Silveira Neto, A., Figueira da Silva, L.F. and Mura, A., 2015, "Influence of synthetic inlet turbulence on the prediction of low Mach number flows", *Computers & Fluids*, Vol. 106, pp. 135-153.

11. Celis, C. and Figueira da Silva, L.F., 2015, "Study of mass consistency LES/FDF techniques for chemically reacting flows", *Combustion Theory and Modelling* (Available online, DOI: 10.1080/13647830.2015.1048828).

12. Orbegoso, E.M., Figueira da Silva, L.F. and Novgorodcev Jr., A.R., 2011, On The Predictability of Chemical Kinetics for the Description of the Combustion of Simple Fuels, *Journal of the Brazilian Society of Mechanical Sciences and Engineering*, Vol. 33, pp. 492-505.

13. Appel, J., Bockhorn, H. and Frenklach, M., 2000, "Kinetic modeling of soot formation with detailed chemistry and physics: laminar premixed flames of C2 hydrocarbons", *Combustion and Flame*, Vol. 121, pp. 122-136.

14. El Bakali, A., Pillier, L., Desgroux, P., Lefort, B., Gasnot, L., Pauwles, J.F., and da Costa, I., 2006, "NO prediction in natural gas flames using GDF-Kin®3.0 mechanism NCN and HCN contribution to prompt-NO formation", *Fuel*, Vol. 85, pp. 896-909.

15. Le Cong, T. and Dagaut, P., 2008, "Effect of Water Vapor on the Kinetics of Combustion of Hydrogen and Natural Gas: Experimental and Detailed Modeling Study", *Proceedings of GT2008, ASME Turbo Expo 2008, Power for Land, Sea and Air*, Berlin, Germany.

16. Konopka, T.F., 2014, "Estudo comparativo de modelos de cinética química detalhada de precursores de fuligem para combustão etileno/ar e metano/ar", MSc Dissertation, Pontifícia Universidade Católica do Rio de Janeiro, Brazil.

17. Lu, T. and Law, C.K., 2005, "A directed relation graph method for mechanism reduction", *Proceedings of the Combustion Institute*, Vol. 30, pp. 1333-1341.

18. Lam, S.H., 1985, "Singular perturbation for stiff equations using numerical methods", In *Recent Advances in the Aerospace Sciences*, Corrado Casci (Ed.), Plenum Press, New York and London, pp.3-20.

19. Goussis, D.A., Lam, S.H. and Gnoffo, P.A., 1990, "Reduced and simplified chemical kinetics for air dissociation using computational singular perturbation", *AIAA 28th Aerospace Sciences Meeting*, Reno (Nevada), US.

20. Lam, S.H., 1993, "Using CSP to understand complex chemical kinetics", *Combustion Science and Technology*, Vol. 89, pp. 375-404.

21. Massias, A., Diamantis, D., Mastorakos, E. and Goussis, D.A., 1999, "An algorithm for the construction of global reduced mechanisms with CSP data", *Combustion and Flame*, Vol. 117, pp. 685-708.

22. Bilger, R.W., Stårner, S.H. and Kee, R.J., 1990, "On reduced mechanisms for methane-air combustion in nonpremixed flames", *Combustion and Flame*, Vol. 80, pp. 135-149.

23. Chen, J.Y. and Dibble, R.W., 1991, "Application of reduced chemical mechanisms for prediction of turbulent nonpremixed methane jet flames", In *Reduced Kinetic Mechanisms and Asymptotic Approximations for Methane-Air Flames*, M.D. Smooke (Ed.), Lecture Notes in Physics, Vol. 384, pp. 193-226.

24. Jones, W.P. and Lindstedt, R.P., 1988, "Global reaction schemes for hydrocarbon combustion", *Combustion and Flame*, Vol. 73, pp. 233-249.

25. Peters, N. and Kee, R.J., 1987, "The computation of stretched laminar methane-air diffusion flames using a reduced four-step mechanism", *Combustion and Flame*, Vol. 68, pp. 17-29.

26. Peters, N. and Williams, F.A., 1987, "The asymptotic structure of stoichiometric methane-air flames", *Combustion and Flame*, Vol. 68, pp. 185-207.

27. Sung, C.J., Law, C.K. and Chen, J.Y., 1998, "An augmented reduced mechanism for methane oxidation with comprehensive global parametric validation", *Symposium (International) on Combustion*, Vol. 27, pp. 295-304.

28. Sung, C.J., Law, C.K. and Chen, J.Y., 2001, "Augmented reduced mechanisms for NO emission in methane oxidation", *Combustion and Flame*, Vol. 125, pp. 906-919.

29. Caetano, N. and Figueira da Silva, L.F., 2015, "A comparative experimental study of turbulent non premixed flames stabilized by a bluff-body burner", *Experimental Thermal and Fluid Science*, Vol. 63, pp. 20-33.

30. Egusquiza, J.C., and Figueira da Silva, L.F., 2013, Turbulent non-premixed ethanol-air flame experimental study using laser diagnostics, *Journal of the Brazilian Society of Mechanical Sciences and Engineering*, Vol. 35, pp. 177-188.

31. Roque, A.O. and Figueira da Silva, L.F., 2015, Characterization of multi-jet turbulent flames in cross flow using stereo-PIV and OH-PLIF, *Fire Safety Journal*, Vol. 78, pp. 44-54.

32. Lefebvre, A.H., 1998, *Gas Turbine Combustion*, 2 Ed., Taylor & Francis, Philadelphia, PA, US.

33. GRI-Mech, 2014, <http://combustion.berkeley.edu/gri-mech/>.

34. Xu, J. and Pope, S.B., 2000, "PDF calculations of turbulent nonpremixed flames with local extinction", *Combustion and Flame*, Vol. 123, pp. 281–307.

35. Barlow, R.S. and Frank, J.H., 1998, "Effects of turbulence on species mass fractions in methane/air jet flames", *Proceedings of the Combustion Institute*, Vol. 27, pp. 1087-1095.

36. Mallampalli, H.P., Fletcher, T.H. and Chen, J.Y., 1998, "Evaluation of CH4/NOx reduced mechanisms used for modeling lean premixed turbulent combustion of natural gas", *Journal of Engineering for Gas Turbines and Power*, Vol. 120, pp. 703–712.

37. Yilmaz, S.L., 2013, *Private Communication*, Center for Simulation and Modeling, University of Pittsburgh.

38. Sandia National Laboratories, 2014, <http://www.sandia.gov/>.

39. Cao, R.R. and Pope, S.B., 2005, "The influence of chemical mechanisms on PDF calculations of nonpremixed piloted jet flames", *Combustion and Flame*, Vol. 143, pp. 450–470.

40. Sung, C.J., 2014, *Private Communication*, Mechanical Engineering Department, University of Connecticut.

41. Glarborg, P., Kee, R.J., Grcar, J.F. and Miller, J.A., 1986, *PSR: A Fortran program for modeling well-stirred reactors*, Tech. Rep. SAND86-8209, Sandia National Laboratories, Livermore, CA, US.

42. Kee, R.J., Grcar, J.F., Smooke, M.O. and Miller, J.A., 1985, *PREMIX: A Fortran program for modeling steady laminar one-dimensional premixed flames*, Tech. Rep. SAND85-8240, Sandia National Laboratories, Albuquerque, NM, US.

43. Law, C.K., 2006, *Combustion Physics*, Cambridge University Press, New York, US.

44. Lindstedt, P.R., 1994, Simplified Soot Nucleation and Surface Growth Steps for Non-Premixed Flames, in *Soot Formation in Combustion, Mechanisms and Models*, Bockhorn, H. (Ed.), Springer-Verlag, Berlin, Germany.

45. Jones, W.P. and Whitelaw, J.H., 1982, Calculation methods for reacting turbulent flows: A review, *Combustion and Flame*, Vol. 48, pp. 1-26.

46. Fox, R.O., 2003, *Computational Models for Turbulent Reacting Flows*, Cambridge University Press, Cambridge, UK.

47. Sabel'nikov, V. and Figueira da Silva, L.F., 2002, "Partially stirred reactor: study of the sensitivity of the Monte-Carlo simulation to the number of stochastic particles with the use of a semi-analytic, steady-state, solution to the PDF equation", *Combustion and Flame*, Vol. 129, pp. 164-178.

48. Orbegoso, E.M. and Figueira da Silva, L.F., 2009, "Study of stochastic mixing models for combustion in turbulent flows", *Proceedings of the Combustion Institute*, Vol. 32, pp. 1595-1603.

49. Celis, C., Moss, B. and Pilidis, P., 2009, "Emissions modelling for the optimisation of greener aircraft operations", *GT2009-59211, Proceedings of the ASME Turbo Expo 2009*, Orlando (Florida), US.

50. Correa, S.M., 1993, "Turbulence-chemistry interactions in the intermediate regime of premixed combustion", *Combustion and Flame*, Vol. 93, pp. 41-60.

51. Correa, S.M. and Braaten, M.E., 1993, "Parallel simulations of partially stirred methane combustion", *Combustion and Flame*, Vol. 94, pp. 469-486.

52. Villermaux, J. and Devillon, J.C., 1972, "Représentation de la coalescence et de la redispersion des domaines de ségrégation dans un fluide par un modèle d'interaction phénoménologique", *Proceedings of the 2nd international symposium on chemical reaction engineering*, New York, US.

53. Dopazo, C. and O'Brien, E.E., 1974, "An approach to the autoignition of a turbulent mixture", *Acta Astronautica*, Vol. 1, pp. 1239-1266.

54. Brookes, S.J. and Moss, J.B., 1999, "Predictions of soot and thermal radiation properties in confined turbulent jet diffusion flames", *Combustion and Flame*, Vol. 116, pp. 486–503.

55. Aksit, I.M. and Moss, J.B., 2006, "A hybrid scalar model for sooting turbulent flames", *Combustion and Flame*, Vol. 145, pp. 231–244.

56. Moss, J.B., 1994, Modelling Soot Formation for Turbulent Flame Prediction, in *Soot Formation in Combustion, Mechanisms and Models*, Bockhorn, H. (Ed.), Springer-Verlag, Berlin, Germany.

57. Pope, S.B. 1997, "Computationally efficient implementation of combustion chemistry using in situ adaptive tabulation", Combustion Theory and Modelling, Vol. 1, pp. 41-63.

58. Cunha Jr, A. and Figueira da Silva, L.F., 2014, "Assessment of a transient homogeneous reactor through in situ adaptive tabulation", *Journal of the Brazilian Society of Mechanical Sciences and Engineering*, Vol. 36, pp. 377-391.

59. Kee, R.J., Rupley, F.M. and Miller, J.A., 1991, *CHEMKIN II: A Fortran chemical kinetics package for the analysis of gas-phase chemical kinetics*, Sandia National Laboratories, Livermore, CA, US.

60. Lawrence Livermore National Laboratory, Center for Applied Scientific Computing, 2016, <http://computation.llnl.gov/casc/sundials/>.

61. Qamar, N.H., Alwahabi, Z.T., Chan, Q.N., Nathan, G.J., Roekaerts, D. and King, K.D., 2009, "Soot volume fraction in a piloted turbulent jet non-premixed flame of natural gas", *Combustion and Flame*, Vol. 156, pp. 1339-134.